

# Unraveling the Spin Coulomb Drag Effect and Its Impact on Spin Transport in the Three-Dimensional Electron Gas

Zhiyi Li<sup>1,\*</sup>, Pengcheng Hou<sup>2,1,\*</sup>, Youjin Deng<sup>1,2,3,†</sup> and Kun Chen<sup>4,5,6‡</sup>

<sup>1</sup> *Department of Modern Physics, University of Science and Technology of China, Hefei, Anhui 230026, China*

<sup>2</sup> *Hefei National Laboratory, University of Science and Technology of China, Hefei 230088, China*

<sup>3</sup> *Hefei National Research Center for Physical Sciences at the Microscale and School of Physical Sciences, University of Science and Technology of China, Hefei 230026, China*

<sup>4</sup> *CAS Key Laboratory of Theoretical Physics, Institute of Theoretical Physics, Chinese Academy of Sciences, Beijing 100190, China*

<sup>5</sup> *Center for Computational Quantum Physics, Flatiron Institute, 162 5th Avenue, New York, New York 10010 and*

<sup>6</sup> *Department of Physics and Astronomy, Rutgers, The State University of New Jersey, Piscataway, NJ 08854-8019 USA*

(Dated: May 21, 2024)

The spin Coulomb drag effect, arising from the exchange of momentum between electrons of opposite spins, plays a crucial role in the spin transport of interacting electron systems. This effect leads to the emergence of a spin mass and the finite lifetime of spin currents, posing challenges for the accurate description of spin dynamics. Using the state-of-the-art Variational Diagrammatic Monte Carlo approach, we investigate the spin-resolved exchange-correlation (XC) kernel in the three-dimensional uniform electron gas. Our analysis reveals a distinct nature in the spin response, characterized by a  $1/q^2$  divergence in the spin XC kernel at finite frequencies. This so-called ultranlocal behavior, stemming from the spin Coulomb drag effect, is absent in the charge channel. By extracting precise values for the spin mass enhancement factor, we observe a trend of increasing enhancement with decreasing electron density. Furthermore, we find compelling evidence for the suppression of spin diffusion at low temperatures, characterized by vanishing inverse relaxation times. These findings deepen our understanding of the intricate relation between the Coulomb interaction and the spin transport, providing valuable insights for the development of accurate density functional approximations and the advancement of spintronics and quantum technologies.

## I. INTRODUCTION

Spin transport in interacting electron systems is a fundamental problem with far-reaching implications for spintronics and quantum technologies. The key challenge in describing spin transport lies in the complex interplay between electron-electron interactions and the non-conservation of spin currents. Unlike charge currents, which are conserved, spin currents can be dissipated through the exchange of momentum between electrons of opposite spins. This dissipation mechanism, known as the spin Coulomb drag effect [1, 2], leads to a friction between the spin currents of different components and gives rise to two major consequences: the generation of a spin mass and the finite lifetime of spin currents.

The spin Coulomb drag effect manifests itself through the emergence of a *spin mass*  $m_s$ , a many-body parameter that determines the spin current carried by a single quasiparticle [3]. In the presence of electron-electron interactions, the spin current carried by a quasiparticle of momentum  $\mathbf{p}$  and spin  $\sigma$  is proportional to  $\mathbf{p}/m_s$ , rather than  $\mathbf{p}/m$ , where  $m$  is the bare electron mass. The spin mass  $m_s$  is larger than both the bare electron mass and

the quasiparticle effective mass  $m^*$ , indicating that interactions have a significant impact on spin transport.

In addition to the spin mass, the spin Coulomb drag effect leads to a dissipation of spin currents, namely the *spin diffusion* phenomenon, characterized by a relaxation time  $\tau_{sd}$  [1]. This relaxation time quantifies the lifetime of spin currents in the presence of electron-electron interactions and plays a crucial role in determining the spin diffusion length and the efficiency of spin transport.

The spin Coulomb drag effect and its consequences have profound implications for the theoretical description of spin transport. In particular, they give rise to a singular structure in the spin-resolved exchange-correlation (XC) kernel of the spin response function [4, 5]. The spin XC kernel denoted as  $K_{XC}^-(\mathbf{q}, \omega)$ , is defined through the spin-spin response function  $\chi_S(\mathbf{q}, \omega)$  and the non-interacting response function  $\chi_0(\mathbf{q}, \omega)$  via the Dyson equation [6]:

$$\chi_S(\mathbf{q}, \omega) = \frac{\chi_0(\mathbf{q}, \omega)}{1 - K_{XC}^-(\mathbf{q}, \omega)\chi_0(\mathbf{q}, \omega)} \quad (1)$$

Here, the superscript ‘-’ in  $K_{XC}^-$  denotes the antisymmetric XC kernel related to the spin channel, while the symmetric XC kernel  $K_{XC}^+$  related to the charge channel will be discussed in the Eq. (5). The spin XC kernel encodes the effects of electron-electron interactions on the spin-spin response and exhibits a singularity  $K_{XC}^- \sim A(\omega)/q^2$  divergence at finite frequencies in

\* These two authors contributed equally to this paper.

† yjdeng@ustc.edu.cn

‡ chenkun@itp.ac.cn

the long-wavelength limit. The  $1/q^2$  singularity in the exchange-correlation (XC) kernel is referred to as *ultranonlocality* in density functional theory (DFT). This concept describes how a finite change in the XC potential can be triggered by an infinitesimally small change in the density of the system [7]. Specifically, the factor  $A(\omega)$  is associated with the spin mass and the relaxation time as,

$$A(\omega) = -\frac{m}{n\tau_{sd}}i\omega - \frac{m_s - m}{m}n\omega^2 + \mathcal{O}(\omega^3), \quad (2)$$

where  $n$  is the density of electrons. This divergence is a direct manifestation of the non-conservation of spin currents and has significant consequences for the development of time-dependent density functional theory (TDDFT) [8, 9].

The ultranonlocality of the spin XC kernel poses severe challenges for the construction of approximate XC functional in TDDFT. Local or semi-local approximations, such as the adiabatic local spin density approximation [10], fail to capture the singular behavior of the kernel and the associated spin mass enhancement, leading to qualitatively incorrect predictions for spin transport. Advanced functionals that incorporate the ultranonlocal dependence of the spin currents and the spin Coulomb drag effect are therefore essential for the accurate description of spin dynamics in interacting systems.

Despite the fundamental importance of the spin mass, the spin diffusion, and their relation to the ultranonlocality of the spin XC kernel, direct numerical evidence of these phenomena has been lacking. Theoretical calculations have been limited to diagrammatic expansions [1] and variational quantum Monte Carlo methods [5, 11, 12], which are restricted to the high-density regime and provide only approximate results. A quantitative understanding of the spin mass enhancement, the spin diffusion relaxation time, and their dependence on electron density has remained elusive, hindering the development of accurate XC functionals for spin transport.

In this paper, we present a systematic study of spin transport in interacting electron systems using the state-of-the-art Variational Diagrammatic Monte Carlo (VDMC) method [13, 14]. Our calculations, spanning over a wide range of electron densities, momenta, and Matsubara frequencies, provide the first direct numerical evidence of the ultranonlocal behavior of the spin-resolved XC kernel, characterized by a  $1/q^2$  divergence at finite frequencies. In addition, we demonstrate the absence of this divergence in the charge response, highlighting the unique nature of many-body effects in the spin channel. Furthermore, we extract precise values for the spin mass enhancement factor and the spin diffusion relaxation time, revealing their dependence on electron density and the suppression of the spin diffusion in the 3D uniform electron gas (UEG) at low temperatures.

Our findings not only deepen the understanding of the interplay between XC effects and spin transport but also provide a quantitative benchmark for the development of advanced XC functionals that accurately capture the ul-

tranonlocal behavior and the spin Coulomb drag effect. These functionals are essential for the reliable description of spin dynamics in interacting systems and the prediction of spin-dependent properties in real materials, which is essential for the further development of technologies in spintronics and quantum computing.

The implications of our work extend beyond the 3D UEG, paving the way for the exploration of spin transport in realistic systems, such as semiconductors, transition metals, and low-dimensional materials. The insights gained from our study can guide the design of novel spintronic devices that exploit the rich interplay between electron-electron interactions and spin dynamics, opening up new avenues for the manipulation and control of spin currents in quantum technologies.

The structure of our paper is as follows. In Sec. I, we introduce the theoretical background of spin transport in interacting electron systems, highlighting the importance of the spin Coulomb drag effect and its consequences, namely the spin mass enhancement and the spin diffusion phenomenon. Sec. II describes the VDMC method and its application to the calculation of the spin-spin response function in the 3D UEG. Our results are presented in two main sections: in Sec. III A, we demonstrate the ultranonlocal behavior of the spin XC kernel and its absence in the charge response; in Sec. III B, we extract the spin mass enhancement factor and the spin Coulomb drag relaxation time, discussing their dependence on electron density and the suppression of the dissipation of the spin currents at low temperatures. In Sec. IV, we summarize our conclusions and discuss the implications of our findings for the development of advanced XC functionals and the understanding of spin transport in realistic systems, as well as the potential impact on the design of spintronic devices.

## II. MODEL & METHOD

We focus on an interacting electron system modeled as a UEG without any disorder. This system consists of electrons uniformly distributed within a homogeneous, positively charged background, interacting via the Coulomb potential. The system is conveniently described by two essential parameters: the density parameter, often referred to as the Wigner-Seitz radius  $r_s = \bar{r}/a_B$ , and the reduced temperature  $\theta = T/T_F$ . Here,  $\bar{r}$  denotes the average interparticle distance,  $a_B$  the Bohr radius, and  $T_F$  is the Fermi temperature. Besides, there are some characteristic constants of the system, such as the Fermi momentum  $k_F$ , the Fermi energy  $E_F$ , and the density of state at the Fermi surface in the non-interacting system  $N_F$ . The Hamiltonian governing the dynamics of this system is expressed as follows:

$$\begin{aligned}
H = & \sum_{\mathbf{k}\sigma} (\mathbf{k}^2 - \mu) \psi_{\mathbf{k}\sigma}^\dagger \psi_{\mathbf{k}\sigma} \\
& + \frac{1}{2} \sum_{\substack{q \neq 0 \\ \mathbf{k}\mathbf{k}'\sigma\sigma'}} \frac{8\pi}{q^2} \psi_{\mathbf{k}+\mathbf{q}\sigma}^\dagger \psi_{\mathbf{k}'-\mathbf{q}\sigma'}^\dagger \psi_{\mathbf{k}'\sigma'} \psi_{\mathbf{k}\sigma}, \quad (3)
\end{aligned}$$

where  $\psi, \psi^\dagger$  are the annihilation and creation operators of a quasi-electron,  $\mu$  is the chemical potential that is controlled by the parameter  $r_s$ , and the Hamiltonian is formulated using Rydberg atomic units.

Addressing the many-body problem of the UEG Hamiltonian poses significant challenges due to the divergences arising from the bare Coulomb interaction in the diagrammatic expansion [15]. To overcome this issue, we employ the Variational Diagrammatic Monte Carlo (VDMC) method [13, 14, 16–23], an advanced field-theoretic approach that offers controlled accuracy. The VDMC method transforms the problem into an equivalent and more appropriate form for the expansion, taking the emergent low-energy physics as the lowest order of the model. This transformation significantly improves the convergence of the expansion with increasing perturbation order.

Within the VDMC framework, the system's action  $S$  is decomposed into a reference action  $S_0$  and a sequence of counterterms, serving as corrections. The Coulomb interaction inherent in the system is replaced by the Yukawa interaction  $8\pi/(q^2 + \lambda)$ , with  $\lambda$  serving as a variational screening parameter. This substitution allows for the representation of physical observables, such as electronic polarization, through a renormalized Feynman diagrammatic series [24, 25], expanding in powers of the Yukawa term. The introduction of the ‘‘polarization’’ counterterm  $\lambda/8\pi$  effectively cancels out large contributions arising from particle-hole fluctuations, expediting the convergence of the diagrammatic series. The parameter  $\lambda$  is subject to iterative optimization to enhance conver-

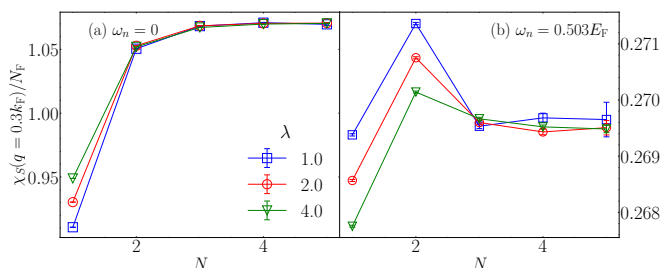


FIG. 1. Spin-spin response function  $\chi_S$  at  $q = 0.3k_F$  versus truncation order  $N$  for  $\theta = 0.01$  and  $r_s = 1$ . Panel (a) shows the static case, and Panel (b) shows the case with  $\omega_n = 0.503E_F$ . All  $\lambda$  choices lead to the same extrapolated value, and the optimal  $\lambda$  for the fastest convergence is about 2.0 for  $\omega_n = 0$  and 4.0 for  $\omega_n = 0.503E_F$ . Here  $k_F$  denotes the Fermi momentum,  $E_F$  denotes the Fermi energy and  $N_F$  denotes the density of state at the Fermi surface in the non-interacting system.

gence [26].

The computational framework of VDMC also incorporates chemical potential counterterms to preserve the electron density at each expansion order. Based on a self-consistent Hartree-Fock (HF) solution for the Green's function, the diagrammatic series is further simplified by omitting Fock-type self-energy insertions. We optimize the electron potential  $v_{\mathbf{k}}$  by inserting the GW-type self-energy, the Fock subdiagram, as the zeroth-order of the effective potential into the bare electron propagator. For higher orders of  $v_{\mathbf{k}}$ , we add chemical-potential counterterms to fix the Fermi surface at each order, ensuring that the electron density remains unchanged order by order, in accordance with the Luttinger theorem.

High-order diagrams are efficiently evaluated through a Monte Carlo method employing importance sampling, with the sampling efficiency optimized using a computational graph representation of the diagrams [23, 27]. The VDMC methodology has been successfully applied to explore various properties of the UEG, including the static and dynamic exchange-correlation kernel [13, 28, 29], the effective mass [14], and the behavior of the electron gas under extreme conditions [30]. By optimizing the diagrammatic expansion, VDMC achieves reliable infinite-order results for any quantity without the need for a large truncation order  $N$ , significantly reducing computational costs while ensuring rapid and precise convergence for high-order calculations of physical observables.

In our investigation, we employ VDMC to evaluate the imaginary-time spin-spin correlation function  $\chi_S(q, \tau) = \langle \mathcal{T} \hat{s}_z(q, \tau) \hat{s}_z(0) \rangle$  in the thermodynamic limit. Subsequent Fourier transformation yields the correlation function in Matsubara frequency space. We then compare the dynamical spin correlation function with theoretical predictions given by Eq.(1) and Eq. (2) to probe the real-frequency dynamics of the spin-spin response function.

To validate the VDMC methodology, we calculate the spin-spin response function  $\chi_S$  at  $r_s = 1, \theta = 0.01, q = 0.3k_F$  up to the fifth diagrammatic order. Figure 1 illustrates rapid numerical convergence of  $\chi_S$  in the vicinity of the optimal  $\lambda$  for two characteristic Matsubara frequencies  $\omega = 0$  and  $\omega = 0.503E_F$ . This confirms VDMC's capability for high-precision, high-order calculations.

### III. RESULTS

We perform extensive VDMC simulations for 3D UEG systems with  $r_s = 0.5, 1.0, 2.0$  at temperatures  $\theta = 0.025, 0.01$ , measuring the spin-resolved response function  $\chi_S$  for momenta  $q$  within  $0.5k_F$  and Matsubara frequencies  $\omega_n \leq E_F$ . Figure 2 shows the collapse of  $\chi_S(i\omega_n, \theta = 0.025)$  and  $\chi_S(i\omega_n, \theta = 0.01)$  onto the same curve for a given  $q$ , indicating that these temperatures are sufficiently low to converge to the zero-temperature limit. Consequently, we focus on simulations at  $\theta = 0.01$  to obtain a denser frequency grid for detailed study of the spin response characteristics.

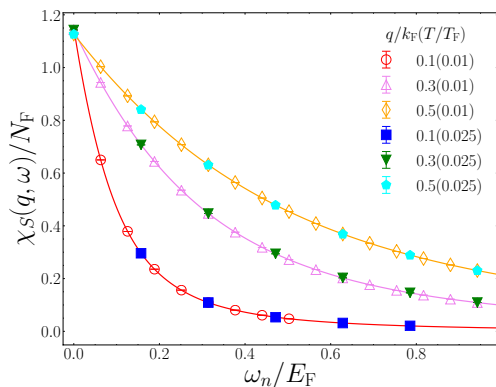


FIG. 2. Spin-spin response function  $\chi_S$  as  $\omega$  increases for different temperatures ( $\theta = 0.025, 0.01$ ) with varying  $q$  of the UEG system ( $r_s = 1.0$ ), indicating that the temperatures used in our simulations are effectively zero.

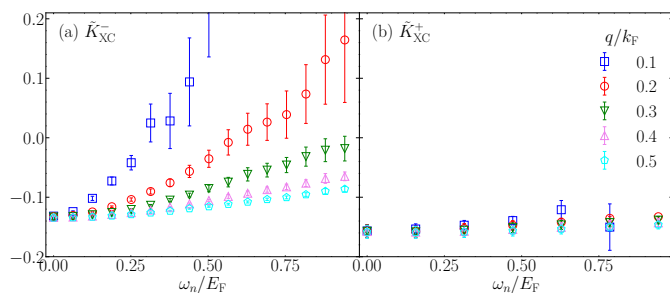


FIG. 3. (a) Spin exchange-correlation (XC) kernel with ( $r_s = 1, \theta = 0.01$ ). They show that the dynamic  $K_{XC}^-$  exhibits a universal divergence in the small- $q$  limit. (b) Charge XC kernel as  $\omega$  increases with various  $q$  with ( $r_s = 1, \theta = 0.025$ ), showing that  $K_{XC}^+$  converges in the small- $q$  limit. Here  $\tilde{K}_{XC}^\pm := K_{XC}^\pm N_F$  is the reduced XC kernel.

### A. Ultranonlocality in the Spin Channel

A key manifestation of many-body effects in the spin response of the 3D UEG caused by the spin Coulomb drag is the ultranonlocal behavior of the dynamic XC kernel  $K_{XC}^-$ . This ultranonlocality, often referred to as the ‘ultranonlocality problem’ in time-dependent spin-density-functional theory [4], is characterized by a divergence of  $K_{XC}^-$  in the small- $q$  limit at finite frequencies.

To investigate this ultranonlocal behavior, we compute  $K_{XC}^-$  through the spin-spin response function  $\chi_S$  and the non-interacting response function  $\chi_0$  using

$$K_{XC}^- = \frac{1}{\chi_0} - \frac{1}{\chi_S}. \quad (4)$$

Figure 3(a) shows the dimensionless  $K_{XC}^-$  as a function of  $\omega_n$  for different momenta at  $r_s = 1.0$ . Apart from the static case ( $\omega_n = 0$ ),  $K_{XC}^-$  increases rapidly as  $q$  approaches zero for a given frequency, clearly demonstrating the ultranonlocal behavior.

To highlight the uniqueness of this behavior in the spin response, we compare it with the charge XC kernel  $K_{XC}^+$ ,

defined as

$$K_{XC}^+ = \frac{1}{\chi_0} - \frac{1}{\chi_{nn}}, \quad (5)$$

where  $\chi_{nn}(q, \tau) = \langle \mathcal{T} \hat{n}(q, \tau) \hat{n}(0) \rangle$  is the density-density response function. Figure 3(b) shows that  $K_{XC}^+$  saturates to a constant in the small- $q$  region, in stark contrast to the ultranonlocal behavior of  $K_{XC}^-$ . This comparison reveals distinct behaviors in the interactions between electrons of different spins, with the ultranonlocality being a unique feature of the spin response. Furthermore, As one can see later in Fig. 4, the ultranonlocal behavior of  $K_{XC}^-$  is consistently observed at different electron densities ( $r_s = 0.5, 1.0$ , and  $2.0$ ), substantiating its universality in the 3D UEG.

Importantly, our analysis of the singular behaviors of the XC kernel, as expressed in Eq. (2), can be carried out in the Matsubara frequency representation  $\omega_n$  at the effective zero temperature. This is made possible by the application of the Wick rotation, a technique that performs an analytical continuation from real frequencies to imaginary frequencies via the transformation  $\omega + i0^+ \rightarrow i\omega_n$ . The Wick rotation is a powerful tool in quantum field theory and many-body physics, allowing for the calculation of real-time quantities using imaginary-time formalisms [31].

The applicability of the Wick rotation in our case is justified by the fact that the XC kernel is analytic in the upper half of the complex frequency plane [6]. This analyticity property ensures that the imaginary-frequency representation contains the same information as the real-frequency one. Moreover, the Matsubara formalism is particularly advantageous for numerical calculations, as it avoids the singularities and branch cuts that may appear in the real-frequency domain [32].

Applying the Wick rotation to Eq. (2), we obtain:

$$A(\omega_n) = \frac{m}{n\tau_{sd}} \omega_n + \left( \frac{m_s}{m} - 1 \right) \frac{m}{n} \omega_n^2 + \mathcal{O} \left( \left( \frac{\omega_n}{E_F} \right)^3 \right), \quad (6)$$

where the first two terms of interest are exactly real. These terms capture the leading contributions to the ultranonlocal behavior at low frequencies and relate the ultranonlocality to two fundamental properties of spin transport: the spin Coulomb drag effect and the spin mass enhancement.

To investigate the structure of the spin XC kernel, we perform a least-square fit of our numerical data to the analytical ansatz:

$$K_{XC}^-(q, i\omega_n) \xrightarrow{q \rightarrow 0, i\omega_n \ll E_F} \frac{A(i\omega_n)}{q^2} + B + \mathcal{O}(q^2, i\omega_n), \quad (7)$$

where  $B$  is a constant. This ansatz captures the leading terms in the small- $q$  limit of the XC kernel at finite but small Matsubara frequencies. To facilitate the fitting procedure, we introduce the dimensionless XC kernel  $\tilde{K}_{XC}^- := K_{XC}^- N_F$  and the dimensionless momentum

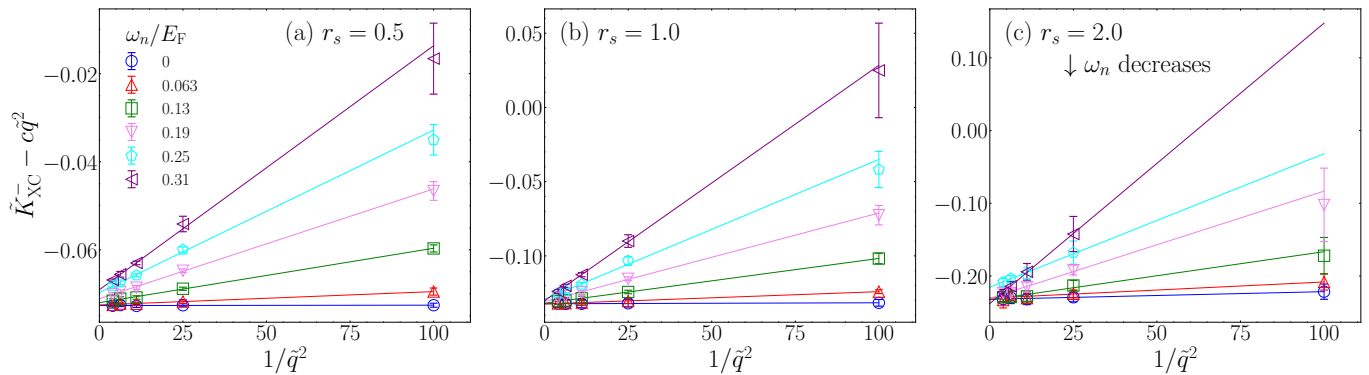


FIG. 4. The reduced XC kernel  $\tilde{K}_{\text{XC}}^-$  excluding the  $\mathcal{O}(\tilde{q}^2)$  term versus  $1/\tilde{q}^2$  ( $\tilde{q} = q/k_{\text{F}}$ ) with various frequency  $\omega_n$  for (a)  $r_s = 0.5$ , (b)  $r_s = 1.0$  and (c)  $r_s = 2.0$ . The slope of the solid lines  $a$  and the parameter  $c$  is derived by fitting Eq. (8) for each frequency. It implies that there is a  $1/q^2$ -divergence of the spin XC kernel, which demonstrate the ultranlocal behaviors in the spin response.

$\tilde{q} := q/k_{\text{F}}$ . We then perform the fit using the following equation:

$$\tilde{K}_{\text{XC}}^- = \frac{a}{\tilde{q}^2} + b + c\tilde{q}^2, \quad (8)$$

where  $a(\omega_n)$ ,  $b(\omega_n)$ , and  $c(\omega_n)$  are frequency-dependent fitting parameters.

The fitting is carried out for each Matsubara frequency  $\omega_n$  within the range  $0 \leq \omega_n \leq 0.314E_{\text{F}}$  and for three different electron densities corresponding to  $r_s = 0.5, 1,$  and  $2$ . The obtained fitting parameters are reported in Table I.

$r_s$	$\omega/E_{\text{F}}$	$a$	$b$	$c$
0.5	0.000	0.000 001(2)	-0.072 67(14)	-0.009 2(9)
	0.063	0.000 030(4)	-0.072 5(2)	-0.008 4(10)
	0.126	0.000 124(5)	-0.072 0(2)	-0.009 4(14)
	0.188	0.000 250(11)	-0.071 1(3)	-0.011(2)
	0.251	0.000 37(3)	-0.069 7(7)	-0.014(4)
	0.314	0.000 55(4)	-0.069 1(7)	-0.013(2)
1.0	0.000	0.000 006(3)	-0.132 2(2)	-0.010 6(14)
	0.063	0.000 083(1)	-0.132 37(4)	-0.008 8(3)
	0.126	0.000 301(2)	-0.131 87(8)	-0.010 3(5)
	0.188	0.000 60(3)	-0.130 9(9)	-0.012(5)
	0.251	0.000 98(11)	-0.130(3)	-0.013(12)
	0.314	0.001 59(3)	-0.130 1(6)	-0.009(2)
2.0	0.000	0.000 10(2)	-0.232(2)	0.022(7)
	0.063	0.000 22(7)	-0.230(4)	0.007(23)
	0.126	0.000 66(14)	-0.233(4)	0.03(2)
	0.188	0.001 4(2)	-0.231(6)	0.02(3)
	0.251	0.001 8(4)	-0.215(8)	-0.03(3)
	0.314	0.003 8(2)	-0.238(3)	0.053(10)

TABLE I. Fitting result of  $K_{\text{XC}}^-$  for various frequency via Eq. (8) for various  $r_s$ .

To validate the consistency of our numerical results with the analytical ansatz, we examine the behavior of the modified XC kernel,  $\tilde{K}_{\text{XC}}^- - c(\omega_n)\tilde{q}^2$ , which excludes the regular  $\mathcal{O}(q^2)$  term. As shown in Fig. 4, this modified XC kernel exhibits a clear linear dependence on  $1/q^2$  for

various  $\omega_n$  values, confirming the presence of the  $1/q^2$ -dominant term in the ultranlocal behavior of the 3D UEG, as predicted by the theory.

The slopes of the linear fits in Fig. 4, represented by the solid lines of different colors, correspond to the fitting parameter  $a(\omega_n)$  for each Matsubara frequency. Notably, the slopes increase monotonically with increasing frequency, indicating that  $a(\omega_n)$  is a monotonically increasing function of  $\omega_n$  within the low-frequency domain, without any divergence.

The comprehensive analysis of our numerical data through the least-square fitting procedure demonstrates the consistency of the ultranlocal behavior of the spin XC kernel in the 3D UEG with the analytical predictions. The frequency-dependent fitting parameters obtained from this analysis will serve as a foundation for the investigation of the spin diffusion and the spin mass enhancement in the following subsection.

## B. Spin Mass Enhancement and Spin Diffusion Phenomenon

The frequency-dependent fitting parameter  $a(\omega_n)$ , obtained from the analysis of the ultranlocal behavior of the spin XC kernel, provides valuable insights into two fundamental properties of spin transport in the 3D UEG: the spin mass enhancement and the spin diffusion phenomenon. These properties are encapsulated in the low-frequency expansion of  $a(\omega_n)$ , as indicated by Eq. (6).

To quantitatively investigate these properties, we perform a least-square fit of  $a(\omega_n)$  using a second-order polynomial ansatz in terms of the reduced Matsubara frequency  $\tilde{\omega} := \omega/E_{\text{F}}$ :

$$a(\omega) = a_0 + a_1\tilde{\omega} + a_2\tilde{\omega}^2 + O(\tilde{\omega}^3). \quad (9)$$

The constant term  $a_0$  is set to zero, as the XC kernel  $K_{\text{XC}}^-$  converges for different momenta  $q$  in the static limit ( $\omega = 0$ ), as shown in Fig. 3. The fitting coefficients  $a_1$  and

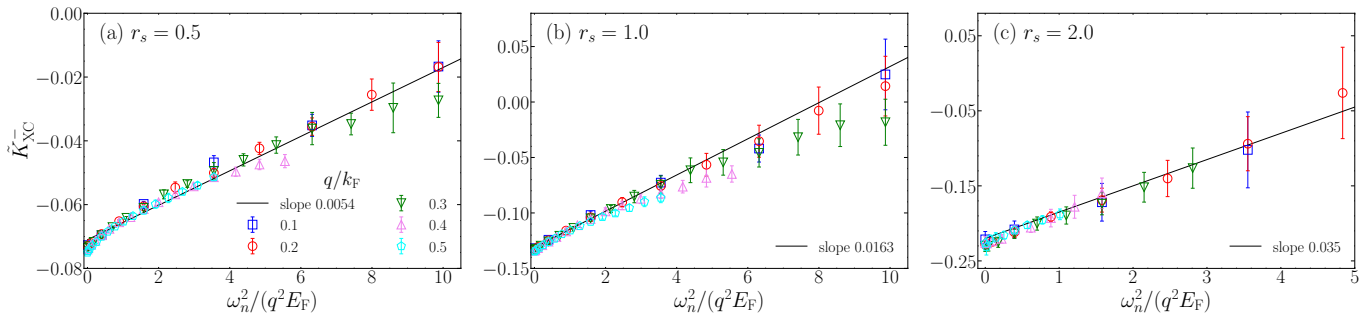


FIG. 5. The reduced XC kernel versus  $\omega_n^2/q^2$  for various  $r_s$ : (a) 0.5, (b) 1.0, (c) 2.0. The slope of the solid lines represent the parameter  $a_2$ , which implies the spin mass renormalization term is dominant at low temperature while the spin diffusion is vanishing.

$a_2$  are determined for three different electron densities, corresponding to  $r_s = 0.5, 1.0,$  and  $2.0$ , and are reported in Table II.

By comparing the low-frequency expansion of  $a(\omega_n)$  in Eq. (9) with the analytical expression in Eq. (6), we can extract the spin diffusion relaxation time  $\tau_{sd}$  arising from the spin Coulomb drag effect and the dimensionless spin mass enhancement factor  $m_s/m$ :

$$\tau_{sd} = \frac{mE_F N_F}{na_1 k_F^2}, \quad (10)$$

$$\frac{m_s}{m} = \frac{nk_F^2 a_2}{mN_F E_F^2} + 1. \quad (11)$$

The values of  $\tau_{sd}$  and  $m_s/m$ , computed using the fitting coefficients, are also listed in Table II for each  $r_s$ .

$r_s$	$a_1(10^{-4})$	$a_2$	$E_F^{-1}/\tau_{sd}(10^{-3})$	$m_s/m$
0.5	2.5(10)	0.0054(6)	3(1)	1.0072(8)
1.0	3.0(5)	0.0163(6)	4.0(6)	1.0217(8)
2.0	10(21)	0.035(8)	-	1.047(10)

TABLE II. Fitting coefficients  $a_1$  and  $a_2$  extracted from the low-frequency expansion of  $a(\omega_n)$  for different  $r_s$  values, along with the derived spin Coulomb drag relaxation time  $\tau_{sd}$  (normalized by the inverse Fermi Energy  $E_F^{-1}$ ) and the spin mass enhancement factor  $m_s/m$ .

The spin mass enhancement factor  $m_s/m$  quantifies the renormalization of the electron mass due to many-body effects in the spin channel. Our numerical analysis yields highly precise values for the spin mass enhancement factor  $m_s/m$ : 1.0072(8) for  $r_s = 0.5$ , 1.0217(8) for  $r_s = 1.0$ , and 1.047(10) for  $r_s = 2.0$ . These results represent a significant advancement in the quantitative understanding of many-body effects in the spin channel. Notably, our findings for  $r_s = 1.0$  and  $2.0$  are in consistent with the theoretical predictions of  $m_s/m = 1.02$  and  $1.06$ , respectively, as reported in Ref. [3], but with substantially improved precision. The enhanced precision achieved in our calculations enables a more accurate exploration of spin-related phenomena in interacting electron systems and facilitates more stringent comparisons

between theoretical predictions and experimental observations. Furthermore, our results reveal a clear trend of increasing spin mass enhancement with decreasing electron density (increasing  $r_s$ ), suggesting that many-body effects become more pronounced in the strongly correlated regime.

The relaxation time of the spin diffusion  $\tau_{sd}$  characterizes the decay of spin currents due to electron-electron interactions. In the low-temperature limit,  $\tau_{sd}$  is expected to diverge in the 3D UEG, as the phase space for electron-electron scattering vanishes [1, 6]. Our numerical results confirm this behavior, as the ratio of the inverse Fermi energy to  $\tau_{sd}$ , is found to be of the order of  $10^{-3}$  for  $r_s = 0.5$  and  $1.0$ . For  $r_s = 2.0$ , the uncertainty in  $a_1$  exceeds its value, making a reliable determination of  $\tau_{sd}$  challenging. Nevertheless, the overall trend suggests that  $1/\tau_{sd}$  approaches zero as the temperature tends to zero, consistent with the theoretical expectation of vanishing spin diffusion in the 3D UEG at zero temperature.

The dominance of the spin mass enhancement over the dissipation of the spin current caused by the spin Coulomb drag effect in the low-temperature limit is further corroborated by the plot of the reduced XC kernel  $\tilde{K}_{XC}^-$  as a function of  $\tilde{\omega}^2/\tilde{q}^2$  for different  $r_s$  values, as shown in Fig. 5. The linearity of the plots, with slopes given by the fitting coefficient  $a_2$ , demonstrates that the spin mass renormalization term is the leading contribution to the ultranonlocal behavior of the XC kernel in this regime.

In summary, our numerical analysis of the frequency-dependent fitting parameter  $a(\omega_n)$  provides strong evidence for the presence of spin mass enhancement and the suppression of spin diffusion in the 3D UEG at low temperatures. The precise determination of the spin mass enhancement factor and the confirmation of the vanishing spin diffusion in the zero-temperature limit showcase the power of the VDMC approach in capturing subtle many-body effects in the spin channel. These findings contribute to a deeper understanding of spin transport phenomena in interacting electron systems and serve as a benchmark for future theoretical and computational studies.



#### IV. DISCUSSIONS

In this work, we have employed the Variational Diagrammatic Monte Carlo (VDMC) approach to investigate the spin response of the three-dimensional uniform electron gas (3D UEG) at low temperatures. Our study has focused on the spin Coulomb drag effect through the ultranonlocality behaviors of the spin-resolved exchange-correlation (XC) kernel and its connection to fundamental properties of spin transport, namely the spin mass enhancement and the spin diffusion phenomenon.

Through extensive VDMC simulations, we have computed the spin-spin response function and the associated XC kernel for a wide range of electron densities, momenta, and Matsubara frequencies. Our results clearly demonstrate the presence of a  $1/q^2$  divergence in the spin XC kernel at finite frequencies, confirming the spin Coulomb drag effect predicted by theoretical studies. Remarkably, this singularity is absent in the charge channel, highlighting the unique nature of many-body effects in the spin response.

By fitting our numerical data to an analytical ansatz for the XC kernel, we have extracted the frequency-dependent coefficient of the  $1/q^2$  term, which encodes information about the spin mass enhancement and the dissipation of the spin current. Our analysis has yielded highly precise values for the spin mass enhancement factor, surpassing the accuracy of previous theoretical predictions. Interestingly, we have observed a trend of increasing spin mass enhancement with decreasing electron density, indicating the growing importance of many-body effects in the strongly correlated regime.

Furthermore, our study has provided compelling evidence for the suppression of spin diffusion in the 3D UEG at low temperatures. The extracted relaxation times of the spin current are found to be several orders of magnitude larger than the Fermi time, suggesting that spin currents can persist for extended durations in this system. This finding is consistent with the theoretical expectation of vanishing spin diffusion in the zero-temperature

limit.

The results presented in this work represent a significant advancement in the quantitative understanding of spin-related phenomena in interacting electron systems. The unprecedented precision achieved in our calculations opens up new possibilities for probing subtle many-body effects and facilitates more stringent comparisons between theory and experiment. Moreover, our study highlights the power and versatility of the VDMC approach in tackling challenging problems in the field of spin transport.

Looking ahead, the insights gained from this work can guide the development of more accurate density functional approximations for spin-dependent phenomena, with potential applications in spintronics and quantum technologies. The extension of our methodology to more complex systems, such as multicomponent electron gases and realistic materials, presents exciting avenues for future research.

In conclusion, our comprehensive investigation of the spin response in the 3D UEG has unveiled the intricate interplay between ultranonlocality, spin mass enhancement, and spin Coulomb drag. The precise numerical results and the rigorous theoretical analysis presented here establish a new benchmark for the study of spin transport in interacting electron systems and pave the way for future discoveries in this fascinating field.

#### ACKNOWLEDGEMENTS

Z.L, P.H. and Y.D. were supported by the supported by the National Natural Science Foundation of China (under Grant No. 12275263), the Innovation Program for Quantum Science and Technology (under grant No. 2021ZD0301900), the Natural Science Foundation of Fujian Province of China (under Grant No. 2023J02032). K.C. was supported by National Natural Science Foundation of China under Grants No. 12047503.

- 
- [1] I. D’Amico and G. Vignale, Phys. Rev. B **62**, 4853 (2000).
  - [2] I. D’Amico and C. A. Ullrich, physica status solidi (b) **247**, 235 (2010).
  - [3] Z. Qian, G. Vignale, and D. C. Marinescu, Phys. Rev. Lett. **93**, 106601 (2004).
  - [4] Z. Qian, A. Constantinescu, and G. Vignale, Phys. Rev. Lett. **90**, 066402 (2003).
  - [5] Z. Qian and G. Vignale, Phys. Rev. B **68**, 195113 (2003).
  - [6] G. Giuliani and G. Vignale, *Quantum Theory of the Electron Liquid* (Quantum Theory of the Electron Liquid, 2005).
  - [7] T. Aschebrock, T. Lebeda, M. Brütting, R. Richter, I. Schelter, and S. Kümmel, The Journal of Chemical Physics **159** (2023).
  - [8] E. Runge and E. K. U. Gross, Phys. Rev. Lett. **52**, 997 (1984).
  - [9] P. Elliott, K. Burke, F. Furche, K. Lipkowitz, and T. Cundari, Reviews in Computational Chemistry **26**, 91 (2009).
  - [10] S. V. Halilov, H. Eschrig, A. Y. Perlov, and P. M. Oppeneer, Phys. Rev. B **58**, 293 (1998).
  - [11] D. M. Ceperley and B. J. Alder, Phys. Rev. Lett. **45**, 566 (1980).
  - [12] G. Ortiz and P. Ballone, Phys. Rev. B **50**, 1391 (1994).
  - [13] K. Chen and K. Haule, Nature communications **10**, 1 (2019).
  - [14] K. Haule and K. Chen, Scientific reports **12**, 2294 (2022).
  - [15] K. Van Houcke, I. S. Tupitsyn, and N. V. Prokof’ev, “Diagrammatic monte carlo and gw approximation for

- jellium and hydrogen chain,” in *Handbook of Materials Modeling*, edited by W. Andreoni and S. Yip (Springer International Publishing, Cham, 2020) pp. 435–452.
- [16] N. V. Prokof’ev and B. V. Svistunov, Phys. Rev. Lett. **81**, 2514 (1998).
- [17] N. Prokof’ev and B. Svistunov, Phys. Rev. B **77**, 020408(R) (2008).
- [18] E. Kozik, M. Ferrero, and A. Georges, Phys. Rev. Lett. **114**, 156402 (2015).
- [19] R. Rossi, Phys. Rev. Lett. **119**, 045701 (2017).
- [20] N. Prokof’ev and B. Svistunov, Phys. Rev. Lett. **99**, 250201 (2007).
- [21] R. Rossi, T. Ohgoe, K. Van Houcke, and F. Werner, Phys. Rev. Lett. **121**, 130405 (2018).
- [22] K. Van Houcke, F. Werner, E. Kozik, N. V. Prokof’ev, B. V. Svistunov, M. Ku, A. Sommer, L. Cheuk, A. Schirrotzek, and M. Zwierlein, Nature Physics **8**, 366 (2012).
- [23] P. Hou, T. Wang, D. Cerkoney, X. Cai, Z. Li, Y. Deng, L. Wang, and K. Chen, “Feynman diagrams as computational graphs,” (2024), arXiv:2403.18840 [hep-th].
- [24] R. Rossi, F. Werner, N. Prokof’ev, and B. Svistunov, Phys. Rev. B **93**, 161102 (2016).
- [25] M. E. Peskin, *An introduction to quantum field theory* (CRC press, 2018).
- [26] H. Kleinert, *Path integrals in quantum mechanics, statistics, polymer physics, and financial markets* (World scientific, 2009).
- [27] B.-Z. Wang, P.-C. Hou, Y. Deng, K. Haule, and K. Chen, Phys. Rev. B **103**, 115141 (2021).
- [28] C. A. Kukkonen and K. Chen, Phys. Rev. B **104**, 195142 (2021).
- [29] J. P. F. LeBlanc, K. Chen, K. Haule, N. V. Prokof’ev, and I. S. Tupitsyn, Phys. Rev. Lett. **129**, 246401 (2022).
- [30] P.-C. Hou, B.-Z. Wang, K. Haule, Y. Deng, and K. Chen, Phys. Rev. B **106**, L081126 (2022).
- [31] A. Altland and B. D. Simons, *Condensed matter field theory* (Cambridge university press, 2010).
- [32] H. Bruus and K. Flensberg, *Many-body quantum theory in condensed matter physics: an introduction* (OUP Oxford, 2004).